



Article

Enhanced Ammonia Gas Adsorption through Site-Selective Fluorination of Graphene

Tianbo Duan ¹, Hu Li ^{1,2,3,*}, Lakshya Daukiya ^{4,5}, Laurent Simon ⁴ and Klaus Leifer ^{1,*}¹ Ångström Laboratory, Department of Engineering Sciences, Uppsala University, 75121 Uppsala, Sweden² Shandong Technology Centre of Nanodevices and Integration, School of Microelectronics, Shandong University, Jinan 250101, China³ Shenzhen Research Institute, Shandong University, Shenzhen 518057, China⁴ Institut de Sciences des Matériaux de Mulhouse, CNRS-UMR 7361, 68093 Mulhouse, France⁵ Department of Physics, Indian Institute of Technology Jodhpur, Jodhpur 342037, India

* Correspondence: hu.li@sdu.edu.cn (H.L.); klaus.leifer@angstrom.uu.se (K.L.)

Abstract: Graphene has been widely explored as an ideal platform for gas sensing owing to exceptional properties, such as its atom-thin two-dimensional conjugated structure and large specific surface area. Herein, we report that, by introducing covalent C-F bonds via site-selective ion-beam-induced fluorination, graphene sensing response to ammonia gas can be considerably improved due to the enhanced gas adsorption on the surface of fluorinated graphene. The response to the ammonia gas increased by a factor of eight together with the limit of detection approaching 65 ppb. The absorption kinetics between the ammonia gas and fluorinated graphene were analyzed by using the Langmuir isotherm model and the result shows that the enhanced sensitivity is mainly attributed to the strong binding energy of fluorinated graphene to ammonia gas molecules, which is consistent with previous theoretical predictions.

Keywords: graphene; gas sensing; fluorination; ion beam; ammonia



Citation: Duan, T.; Li, H.; Daukiya, L.; Simon, L.; Leifer, K. Enhanced Ammonia Gas Adsorption through Site-Selective Fluorination of Graphene. *Crystals* **2022**, *12*, 1117. <https://doi.org/10.3390/cryst12081117>

Academic Editor: Igor Neri

Received: 16 July 2022

Accepted: 8 August 2022

Published: 10 August 2022

Publisher's Note: MDPI stays neutral with regard to jurisdictional claims in published maps and institutional affiliations.



Copyright: © 2022 by the authors. Licensee MDPI, Basel, Switzerland. This article is an open access article distributed under the terms and conditions of the Creative Commons Attribution (CC BY) license (<https://creativecommons.org/licenses/by/4.0/>).

1. Introduction

Graphene has been extensively explored as an ideal material in solid state gas sensors due to its atomically thin two-dimensional structure, large specific area and superior electrical properties [1–6]. The past decade has witnessed the advancement of graphene sensors and a number of graphene-based gas sensors have been applied for sensing various gases, such as NO₂ [7,8], NO [9] and CO₂ [10] among others. However, graphene-based ammonia (NH₃) sensors [8,11,12] still attracted considerable interest as the sensor response is relatively much lower (typically less than 5%) when compared to other gas species sensed with pristine graphene [13]. Despite the fact that many methods, such as doping [14], defect insertion [15–17] and surface functionalization [18–21], have been applied, it is still a challenge to improve the sensitivity of graphene-based gas sensors to NH₃. Theoretical studies have predicted that, by covalently introducing fluorine onto graphene surfaces (graphene fluorination), the sensitivity of graphene to NH₃ molecules can be remarkably increased due to the strong binding energy between NH₃ molecules and fluorine sites [22–24]. However, no experimental approach so far has been demonstrated that can verify the hypothesis that such a process can significantly change gas adsorption kinetics. Graphene fluorination can be achieved by a variety of methods, such as chemical exposure to a fluorine-contained substance [25–27], plasma treatment under fluorine-based atmosphere [28–31] and beam induced chemical reactions using XeF₂ as a precursor gas [18]. Among these, the ion-beam-induced functionalization technique displays significant advantages in localizing fluorination sites and controlling fluorine concentrations [18], and could thus provide ideal means for graphene fluorination. The comparison of key parameters for various graphene-based gas sensors for NH₃ detection is shown in Table 1.

Table 1. Graphene-based gas sensors for NH₃ detection at room temperature.

Sensing Materials	Detection Limit	Response Time	Recovery Time	Ref.
CVD-Graphene	500 ppb	6 h	6 h	[8]
F-CVD-Graphene	1 ppm	20 min	20 min	[32]
F-CVD-Graphene	2 ppm	<100 s	<200 s	[22]
F-Graphene	<300 ppm	20 min	-	[33]
PPy/CVD-Graphene	0.1 ppb	10 s	-	[34]

In this work, the ion-beam-induced fluorination method is employed to achieve fluorinated graphene (FG), which is subsequently characterized by Raman spectroscopy, X-ray photoelectron spectroscopy (XPS) and scanning tunnelling microscopy (STM). Systematic NH₃ gas sensing experiments were performed, and our results found that the FG exhibits a high sensing response to NH₃ gas that is considerably enhanced, by a factor of eight, compared to pristine graphene under ambient pressure. According to the Langmuir isotherm model, the limit of detection (LOD) of the obtained FG samples has achieved 65 ppb, which belongs to the class of ultrasensitive gas sensors.

2. Materials and Methods

Commercially available chemical vapor deposited (CVD) graphene on a Cu foil (monolayer, Graphenea, San Sebastián, Spain) was used as the main material in this work. The graphene was transferred to Si substrate covered with 300 nm thick SiO₂ via a PMMA-assisted transfer process [35]. Graphene channels and electrical contacts were fabricated by employing electron beam lithography (NanoBeam nB5, NBL, London, United Kingdom) and low-power O₂ plasma etching (Vision 320 RIE, Advanced Vacuum, Bernin, France) followed by a metal evaporation/lift-off process with Ti (5 nm)/Au (50 nm). The obtained graphene device is shown in Figure 1a (inserted). Subsequently, the graphene is fluorinated by focused ion beam (FIB)-induced functionalization, as described in detail in our previous work [18]. The focused ion beam (1 pA) is scanned across the target surface with an ion dose of 10¹³ ions/cm² under a vacuum of 10⁻⁶ mbar. At the same time, the precursor gas XeF₂ streams out from the gas nozzle to functionalize the graphene. Under the ion beam, the XeF₂ is decomposed and F radicals react with the surrounding C atoms. Since this reaction is more efficient, the F atoms will predominantly bind to the defect sites in the graphene lattice that were caused by the ion bombardment, see Figure 1b. Raman spectroscopy is carried out on a Renishaw inVia spectrometer, with a laser wavelength of 532 nm, to investigate the structural evolution of graphene after ion beam fluorination.

The gas sensing measurements were carried out in a gas sensing probe station under ambient pressure, and the current-voltage (I-V) and current-time (I-t) characteristics of the gas sensing devices were recorded by using a Keithley 6430 sub-femtoamp source meter. Prior to the gas sensing experiment, the chamber was purged with dry N₂ gas for 1 h before introducing the target gas. The gas flow rate was kept to 150 mL/min by a mass flow controller. The sample was applied with a voltage of 50 mV and no gate bias. The gas sensing measurements were performed under an ambient condition with a temperature of 20 °C ± 1 °C and relative humidity 45% ± 3%.

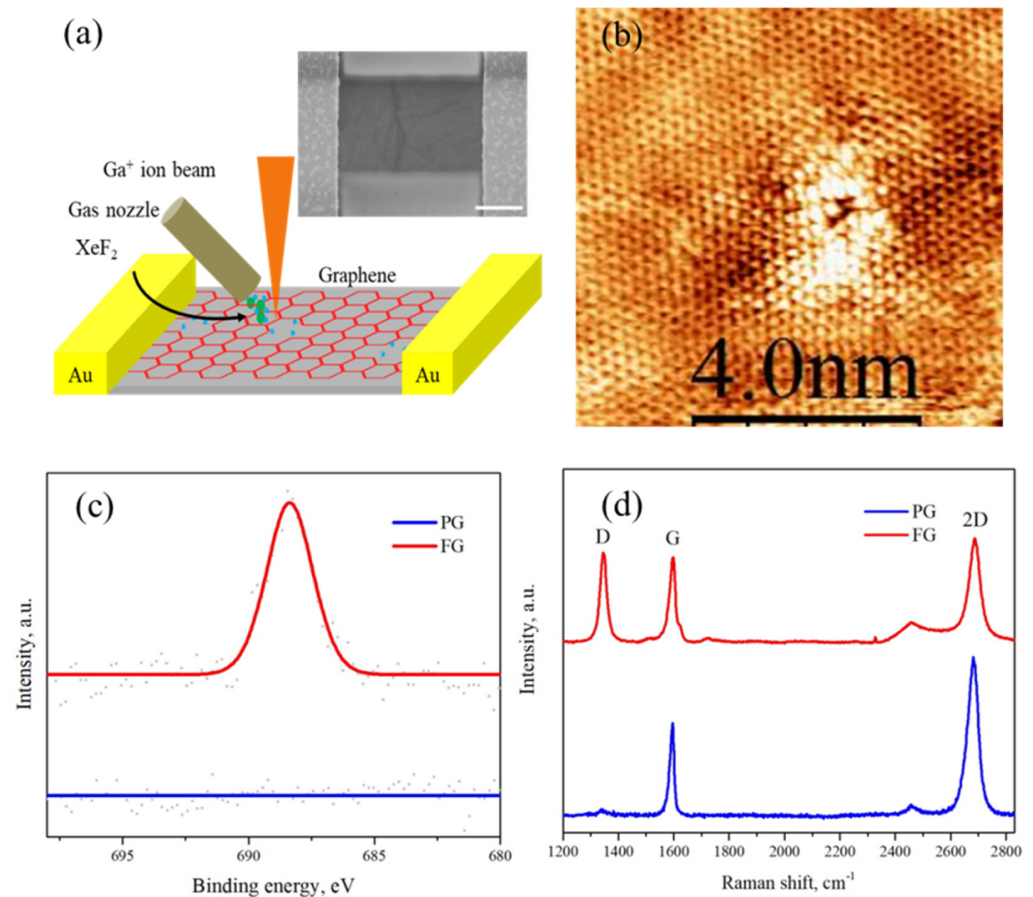


Figure 1. (a) Schematic diagram of the ion beam fluorination process on graphene sensors with two terminals. The scanning electron microscopy image of the device with scale bar of 1 μm is inserted. (b) Scanning tunneling microscopy image of FG. (c) X-ray photoelectron spectroscopy spectra of F1s peaks of PG and FG. (d) Raman spectra of PG and FG.

3. Results

As shown in Figure 1c, the D band appears at $\sim 1350\text{ cm}^{-1}$, which indicates the disorder level [36]. The intensity of this band is significantly weak for pristine graphene, which refers to the good quality of the graphene sample with a level of defects. After graphene fluorination, the increase in the D band in the FG sample is clear to see. Moreover, the decrease in the double resonance 2D band and the broadening of the intrinsic G band is consistent with the previously reported doping effect [37], thus providing strong evidence of the presence of covalent C-F bonds and induced defects on the functionalized graphene. The presence of the covalent C-F bonds is further confirmed by the distinguishable F1s peak in XPS spectra shown in Figure 1c, which were taken with a Quantum 2000 Scanning ESCA system (Physical Electronics, Chanhassen, United States). The atomic fluorine concentration of the FG sample was calculated as $7.5 \pm 0.6\%$ after being corrected with the sensitivity factor and the transmission function of the spectrometer. The fact that C-F bonds are preferably formed in the vicinity of defects during the ion-beam-induced fluorination shown in our previous studies is further confirmed by the STM analysis under vacuum condition, as shown in Figure 1b. In the centre of the STM image, a structural defect is observed. Such defects are only present in high density in graphene layers exposed to the focused ion bombardment and are thus attributed to the damage caused by ion impact. The defect is surrounded by standing waves, which further emphasizes the presence of the defect missing atoms or a covalent bond with a molecule, which shows chemisorption of molecules [38]. The bright contrast in the immediate surroundings of the defect is attributed to the fluorine binding to the pristine graphene. Due to the loss of local conjugation (electron

delocalization along C=C bonds), this part of graphene is rendered less conductive. The larger area scan in Figure S1 also shows that, providing that their density is large enough, dispersed defects/fluorinated areas can be “connected” by the standing waves in between, even if most of the graphene surface remains undamaged, which is consistent with previous reports [18]. The ion dose used to functionalize the graphene sample imaged via STM was chosen to be 10^{13} ions/cm². At this dose, most of the graphene area remains intact while defects are sufficient enough to be localized.

Figure 2a shows normalized conductance response of pristine graphene, defected graphene (DG) and fluorinated graphene (FG) as a function of time under the exposure of 10 ppm NH₃. Here, the sensitivity *S* of the gas sensor is defined as the normalized conductance response as follows:

$$S = \frac{G_{N_2} - G_{NH_3}}{G_{N_2}} \times 100 \%, \quad (1)$$

where G_{N_2} is the initial conductance of the sensor and G_{NH_3} is the final conductance of the sensor after gas exposure. From the comparison, it can be shown that FG exhibits much better response (16.2%) than pristine graphene, with only 2.1% towards NH₃ gas at a concentration of 10 ppm. It is worth mentioning that the gas reaction time in our work was found to be 380 s, much shorter compared to other graphene-based ammonia gas sensors [39–41], which implies a quite fast response time in real applications. It was also found in our work that the recovery time of the FG sample was 780 s with pure N₂ purging, which is slightly increased compared to 600 s for pristine graphene. To better understand the repeatability and stability of the gas sensing experiment, the NH₃ gas sensing was repeated five times in the FG sample, as shown in Figure 2b. It can be clearly observed that the fluorinated graphene has almost the same response, indicating excellent repeatability of performance for the sensor. To further investigate the sensitivity to other gases for the FG sensor, the FG was exposed to CO, which is an acceptor-like gas molecule comparable to NH₃ [7]. The experimental condition was kept unchanged and the concentration of CO was fixed to be 10 ppm. Figure 2d shows that pristine graphene and FG exhibit a nearly negligible response to CO at room temperature, indicating high selectivity to NH₃, which is an important example for environmental sensor applications.

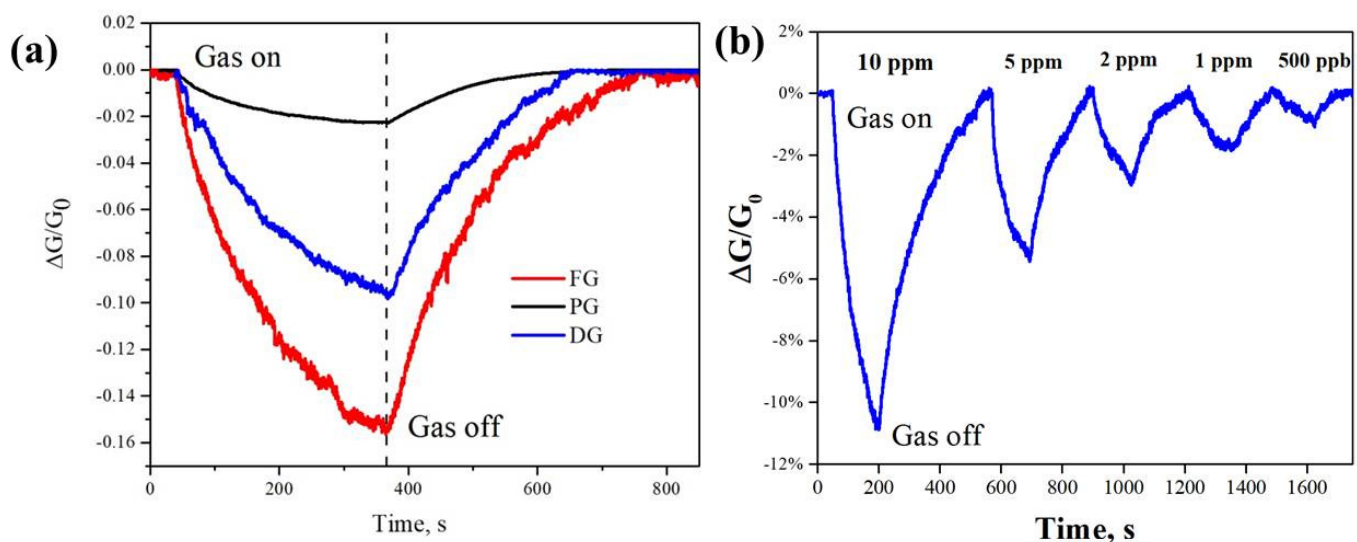


Figure 2. Cont.

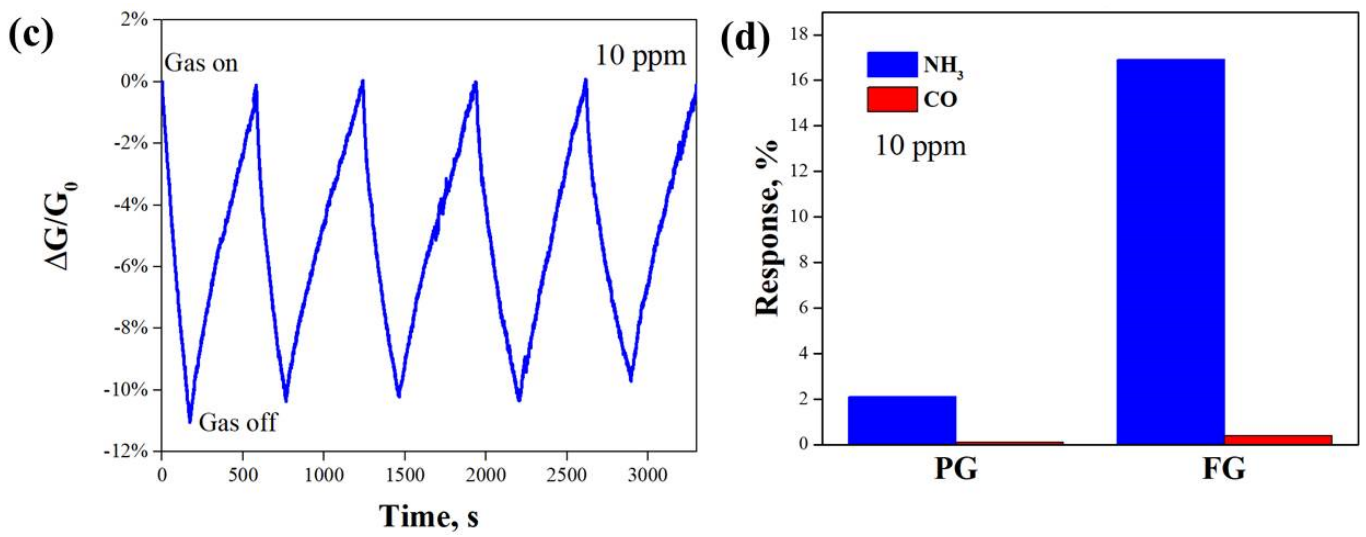


Figure 2. (a) Responses of PG, DG and FG to 10 ppm NH₃ with the same exposure time. (b) Responses of FG devices under different concentration of NH₃ gas under ambient pressure. (c) Repeatability of the FG device to 10 ppm of NH₃ gas. (d) Responses of the PG and FG sensors to NH₃ and CO gases with a concentration of 10 ppm.

4. Discussion

To better understand the gas physisorption kinetics, as well as the limitations regarding detection, the NH₃ sensing experiment of the FG sample with various gas concentrations was performed as shown in Figure 2d. The Langmuir isotherm model was applied to investigate the superior NH₃ gas sensing performance of the fluorinated graphene [42]. The Langmuir isotherm model can be applied for the FG gas sensing mechanism and is summarized by the following formula [43–45]:

$$\frac{P}{S} = \frac{P}{S_0} + \frac{1}{KS_0}, \quad (2)$$

where P is the partial pressure of NH₃, S is the response, K is the equilibrium constant and S_0 is the saturated response. Figure 3a shows the relationship between P and sensitivity. The values of S_0 and K can be derived, from the best linear fit, as 0.19 and 0.40 Pa⁻¹, respectively, as shown in Figure 3a. The sticking probability of NH₃ on FG can be estimated by using the following relation between molecule coverage θ and time t :

$$\theta(t) = \theta(\infty) - \theta(\infty) \exp\left(\frac{-K_a P t}{\theta(\infty)}\right), \quad (3)$$

where $\theta(\infty)$ is molecule coverage at equilibrium under pressure P . K_a is the adsorption constant defined as $K_a = r_a P^{-1} (1 - \theta)^{-1}$ where r_a is the adsorption rate. Since, in the Langmuir isotherm model, sensitivity $S(t)$ is proportional to coverage as $\theta(t) = S(t)/S_0$, then Equation (3) can be written as:

$$S(t) = S(\infty) - S(\infty) \exp\left[\frac{-S_0 K_a P t}{S(\infty)}\right], \quad (4)$$

where $S(\infty)$ is the sensor response at the state of equilibrium. The equilibrium constant K_a can be further written as the function of sticking probability:

$$K_a = \frac{s\sigma}{\sqrt{2\pi k_B m T}}, \quad (5)$$

where σ is the molecular cross-section, m is the mass of NH_3 molecule, k_B is the Boltzmann constant and T is the temperature (300 K). Here, we take σ and m as 10^{-19} m^2 and $7.64 \times 10^{-26} \text{ kg}$, respectively. Figure 2b shows the FG sensor's response to 10 ppm NH_3 under ambient pressure, and the solid line and dashed line represent the experimental and best-fitted value according to Equation (4), respectively. K_a is found to be $7.37 \times 10^{-3} \text{ s}^{-1} \text{ Pa}^{-1}$ according to the fitted value. By substituting the value of K_a into Equation (5), the sticking probability is calculated to be 1.98×10^{-6} . The adsorption energy E_a can be expressed as:

$$E_a = -k_B T \ln\left(\frac{K_a}{\nu K}\right), \quad (6)$$

where ν (10^{12} s^{-1}) is attempt frequency. From the equation above, it can be obtained that the adsorption energy between NH_3 molecules and the fluorinated graphene gas sensor is -0.79 eV (-0.51 eV for pristine graphene). Remarkably, the calculated value is in line with the theoretically predicted values due to the presence of strong hydrogen bonding between the C-F bond and N-H bond [46], leading to a strong sensitivity enhancement of graphene to ammonia gas. Moreover, we also calculate the limit of detection of the FG sensor to NH_3 by $\text{LOD} = 3S_{rms}/l$, where S_{rms} is the root mean square of base noise and l is the slope of response as a function of concentration [47,48]. By substituting S_{rms} , which is calculated to be 6.65×10^{-4} , from the base signal of FG and l ($3.2\% \text{ ppm}^{-1}$) by fitting the linear part of response change as a function of partial pressure (as shown in Figures S2 and S3) into the previous formula, the LOD is calculated to be 64 ppb, which is in the class of ultrasensitive ammonia gas sensors.

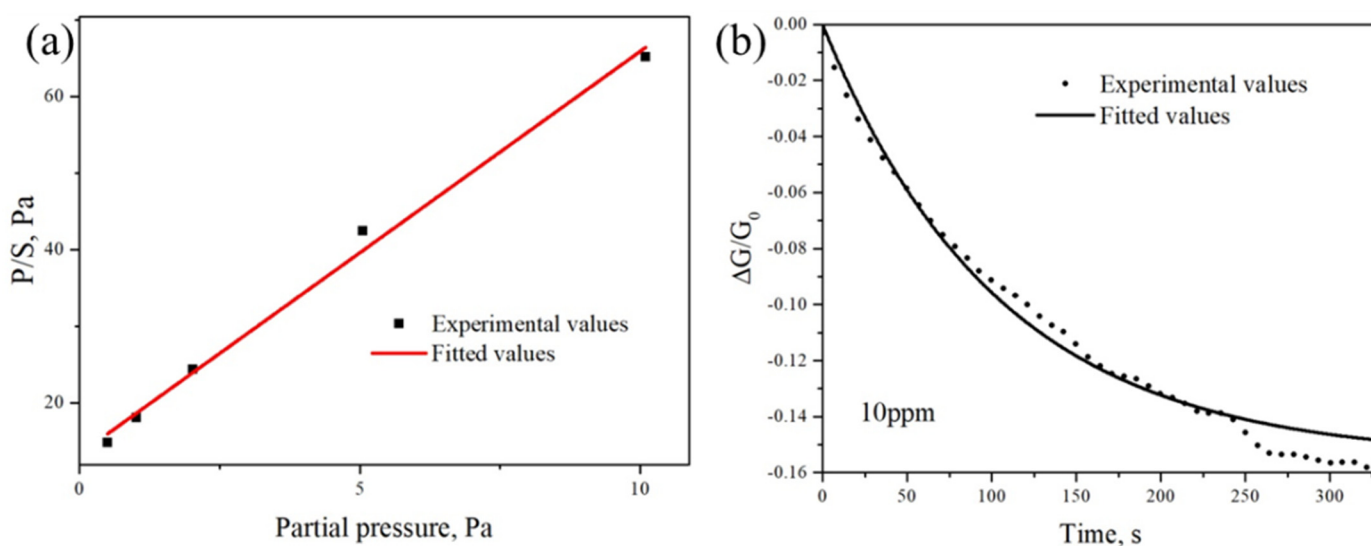


Figure 3. (a) P/S as a function of partial pressure P of NH_3 . The red line is the fitted linear curve. (b) FG sensor response to NH_3 at ambient pressure. The dashed line shows the best fitted curve.

The enhancement of ammonia gas sensing properties of graphene can be attributed to the improved bonding energy between ammonia gas molecules and fluorination sites [23]. The ammonia molecule as the acceptor would attract electrons from graphene, which results in the current decrease. It is also worth mentioning that defects, which are generated in the fluorination process, would also contribute to the gas sensing properties of graphene [17].

5. Conclusions

In this work, we have investigated the effect of fluorination on the NH_3 molecule adsorption properties of graphene through a site-selective ion-beam-induced functionalization technique. Our results show that, compared to pristine graphene, fluorinated graphene exhibits an eight-fold increase in sensing response to NH_3 with LOD down to 64 ppb, which belongs to the class of ultrasensitive ammonia gas sensors. These improved

gas sensing properties are mainly attributed to the enhanced adsorption energy between NH_3 molecules and C-F sites of graphene after fluorination, which is revealed from sensing kinetics by the Langmuir isotherm model. Therefore, our work not only enables an ammonia gas sensor with superior sensitivity, but also contributes to studies involving interactions between gas species and graphene functional groups. The reported approach also has the potential to be employed in a variety of gas detection applications.

Supplementary Materials: The following supporting information can be downloaded at: <https://www.mdpi.com/article/10.3390/cryst12081117/s1>, Figure S1: Large area scanning tunneling microscopy image of fluorinated graphene; Figure S2: Response of fluorinated graphene to NH_3 as a function of partial pressure; Figure S3. F1s XPS spectrum of pristine and fluorinated graphene.

Author Contributions: Conceptualization, T.D., H.L. and K.L.; methodology, H.L. and K.L.; validation, T.D., L.D. and L.S.; formal analysis, T.D., L.D. and L.S.; resources, H.L. and K.L.; data curation, T.D. and H.L.; writing—original draft preparation, T.D., H.L. and K.L.; writing—review and editing, T.D., H.L., L.D., L.S. and K.L.; supervision, H.L. and K.L.; funding acquisition, H.L., L.S. and K.L. All authors have read and agreed to the published version of the manuscript.

Funding: This research was funded by the ÅForsk Foundation (grant number, 20-280), Formas (grant number, 2019-01583), Swedish Research Council (grant number 2016-05259), Olle Engkvist Foundation (grant number, 211-0068), Shandong Provincial Natural Science Foundation (Grant No.: ZR2021QE148 and 2022HWYQ-060), Guangdong Basic and Applied Basic Research Foundation (grant number, 2022A1515011473), Qilu Young Scholar Program of Shandong University (grant number, 11500082063141) and Region Grand Est “NanoteraHertz” grant through the FEDER program.

Data Availability Statement: The data presented in this study are available on request from the corresponding author.

Acknowledgments: Omer Sher and Xiaoxiao Zheng are acknowledged for technical support.

Conflicts of Interest: The authors declare no conflict of interest.

References

1. Geim, A.K.; Novoselov, K.S. The Rise of Graphene. *Nat. Mater.* **2007**, *6*, 183–191. [\[CrossRef\]](#)
2. Li, H.; Zhang, J.; Gholizadeh, A.B.; Brownless, J.; Fu, Y.; Cai, W.; Han, Y.; Duan, T.; Wang, Y.; Ling, H.; et al. Photoluminescent Semiconducting Graphene Nanoribbons via Longitudinally Unzipping Single-Walled Carbon Nanotubes. *ACS Appl. Mater. Interfaces* **2021**, *13*, 52892–52900. [\[CrossRef\]](#)
3. Li, H.; Papadakis, R.; Hussain, T.; Karton, A.; Liu, J. Moiré Patterns Arising from Bilayer Graphene/Graphene Superlattice. *Nano Res.* **2020**, *13*, 1060. [\[CrossRef\]](#)
4. Hunt, B.; Sanchez-Yamagishi, J.D.; Young, A.F.; Yankowitz, M.; LeRoy, B.J.; Watanabe, K.; Taniguchi, T.; Moon, P.; Koshino, M.; Jarillo-Herrero, P.; et al. Massive Dirac Fermions and Hofstadter Butterfly in a van Der Waals Heterostructure. *Science* **2013**, *340*, 1427–1430. [\[CrossRef\]](#)
5. Cai, L.; Zhang, Z.; Xiao, H.; Chen, S.; Fu, J. An Eco-Friendly Imprinted Polymer Based on Graphene Quantum Dots for Fluorescent Detection of p -Nitroaniline. *RSC Adv.* **2019**, *9*, 41383–41391. [\[CrossRef\]](#)
6. Tang, N.; Li, Y.; Chen, F.; Han, Z. In Situ Fabrication of a Direct Z -Scheme Photocatalyst by Immobilizing CdS Quantum Dots in the Channels of Graphene-Hybridized and Supported Mesoporous Titanium Nanocrystals for High Photocatalytic Performance under Visible Light. *RSC Adv.* **2018**, *8*, 42233–42245. [\[CrossRef\]](#)
7. Schedin, F.; Geim, A.; Morozov, S.; Hill, E.; Blake, P.; Katsnelson, M.; Novoselov, K. Detection of Individual Gas Molecules Adsorbed on Graphene. *Nat. Mater.* **2007**, *6*, 652–655. [\[CrossRef\]](#)
8. Yavari, F.; Castillo, E.; Gullapalli, H.; Ajayan, P.M.; Koratkar, N. High Sensitivity Detection of NO_2 and NH_3 in Air Using Chemical Vapor Deposition Grown Graphene. *Appl. Phys. Lett.* **2012**, *100*, 203120. [\[CrossRef\]](#)
9. Singh, G.; Choudhary, A.; Haranath, D.; Joshi, A.G.; Singh, N.; Singh, S.; Pasricha, R. ZnO Decorated Luminescent Graphene as a Potential Gas Sensor at Room Temperature. *Carbon* **2012**, *50*, 385–394. [\[CrossRef\]](#)
10. Fan, X.; Elgammal, K.; Smith, A.D.; Östling, M.; Delin, A.; Lemme, M.C.; Niklaus, F. Humidity and CO_2 Gas Sensing Properties of Double-Layer Graphene. *Carbon* **2018**, *127*, 576–587. [\[CrossRef\]](#)
11. Gautam, M.; Jayatissa, A.H. Graphene Based Field Effect Transistor for the Detection of Ammonia. *J. Appl. Phys.* **2012**, *112*, 064304. [\[CrossRef\]](#)
12. Ben Aziza, Z.; Zhang, Q.; Baillargeat, D. Graphene/Mica Based Ammonia Gas Sensors. *Appl. Phys. Lett.* **2014**, *105*, 254102. [\[CrossRef\]](#)

13. Fowler, J.D.; Allen, M.J.; Tung, V.C.; Yang, Y.; Kaner, R.B.; Weiller, B.H. Practical Chemical Sensors from Chemically Derived Graphene. *ACS Nano* **2009**, *3*, 301–306. [[CrossRef](#)]
14. Mortazavi Zanjani, S.M.; Sadeghi, M.M.; Holt, M.; Chowdhury, S.F.; Tao, L.; Akinwande, D. Enhanced Sensitivity of Graphene Ammonia Gas Sensors Using Molecular Doping. *Appl. Phys. Lett.* **2016**, *108*, 033106. [[CrossRef](#)]
15. Lee, G.; Yang, G.; Cho, A.; Han, J.W.; Kim, J. Defect-Engineered Graphene Chemical Sensors with Ultrahigh Sensitivity. *Phys. Chem. Chem. Phys.* **2016**, *18*, 14198–14204. [[CrossRef](#)]
16. Cagliani, A.; Mackenzie, D.M.A.; Tschammer, L.K.; Pizzocchero, F.; Almdal, K.; Bøggild, P. Large-Area Nanopatterned Graphene for Ultrasensitive Gas Sensing. *Nano Res.* **2014**, *7*, 743–754. [[CrossRef](#)]
17. Hajati, Y.; Blom, T.; Jafri, S.H.M.; Haldar, S.; Bhandary, S.; Shoushtari, M.Z.; Eriksson, O.; Sanyal, B.; Leifer, K. Improved Gas Sensing Activity in Structurally Defected Bilayer Graphene. *Nanotechnology* **2012**, *23*, 505501. [[CrossRef](#)]
18. Li, H.; Daukiya, L.; Haldar, S.; Lindblad, A.; Sanyal, B.; Eriksson, O.; Aubel, D.; Hajjar-Garreau, S.; Simon, L.; Leifer, K. Site-Selective Local Fluorination of Graphene Induced by Focused Ion Beam Irradiation. *Sci. Rep.* **2016**, *6*, 19719. [[CrossRef](#)]
19. Guan, C.; Lv, X.; Han, Z.; Chen, C.; Xu, Z.; Liu, Q. The Adsorption Enhancement of Graphene for Fluorine and Chlorine from Water. *Appl. Surf. Sci.* **2020**, *516*, 146157. [[CrossRef](#)]
20. Cheng, L.; Jandhyala, S.; Mordi, G.; Lucero, A.T.; Huang, J.; Azcatl, A.; Addou, R.; Wallace, R.M.; Colombo, L.; Kim, J. Partially Fluorinated Graphene: Structural and Electrical Characterization. *ACS Appl. Mater. Interfaces* **2016**, *8*, 5002–5008. [[CrossRef](#)]
21. Chen, H.; Chen, Z.; Yang, H.; Wen, L.; Yi, Z.; Zhou, Z.; Dai, B.; Zhang, J.; Wu, X.; Wu, P. Multi-Mode Surface Plasmon Resonance Absorber Based on Dart-Type Single-Layer Graphene. *RSC Adv.* **2022**, *12*, 7821–7829. [[CrossRef](#)] [[PubMed](#)]
22. Zhang, H.; Fan, L.; Dong, H.; Zhang, P.; Nie, K.; Zhong, J.; Li, Y.; Guo, J.; Sun, X. Spectroscopic Investigation of Plasma-Fluorinated Monolayer Graphene and Application for Gas Sensing. *ACS Appl. Mater. Interfaces* **2016**, *8*, 8652–8661. [[CrossRef](#)] [[PubMed](#)]
23. Tadi, K.K.; Pal, S.; Narayanan, T.N. Fluorographene Based Ultrasensitive Ammonia Sensor. *Sci. Rep.* **2016**, *6*, 25221. [[CrossRef](#)]
24. Srivastava, S.; Jain, S.K.; Gupta, G.; Senguttuvan, T.D.; Gupta, B.K. Boron-Doped Few-Layer Graphene Nanosheet Gas Sensor for Enhanced Ammonia Sensing at Room Temperature. *RSC Adv.* **2020**, *10*, 1007–1014. [[CrossRef](#)]
25. Stine, R.; Lee, W.-K.; Whitener, K.E.; Robinson, J.T.; Sheehan, P.E. Chemical Stability of Graphene Fluoride Produced by Exposure to XeF₂. *Nano Lett.* **2013**, *13*, 4311–4316. [[CrossRef](#)]
26. Robinson, J.T.; Burgess, J.S.; Junkermeier, C.E.; Badescu, S.C.; Reinecke, T.L.; Perkins, F.K.; Zalalutdniov, M.K.; Baldwin, J.W.; Culbertson, J.C.; Sheehan, P.E.; et al. Properties of Fluorinated Graphene Films. *Nano Lett.* **2010**, *10*, 3001–3005. [[CrossRef](#)]
27. Mackin, C.; Schroeder, V.; Zurutuza, A.; Su, C.; Kong, J.; Swager, T.M.; Palacios, T. Chemiresistive Graphene Sensors for Ammonia Detection. *ACS Appl. Mater. Interfaces* **2018**, *10*, 16169–16176. [[CrossRef](#)]
28. Wang, B.; Wang, J.; Zhu, J. Fluorination of Graphene: A Spectroscopic and Microscopic Study. *ACS Nano* **2014**, *8*, 1862–1870. [[CrossRef](#)]
29. Chen, M.; Zhou, H.; Qiu, C.; Yang, H.; Yu, F.; Sun, L. Layer-Dependent Fluorination and Doping of Graphene via Plasma Treatment. *Nanotechnology* **2012**, *23*, 115706. [[CrossRef](#)]
30. Nair, R.R.; Ren, W.; Jalil, R.; Riaz, I.; Kravets, V.G.; Britnell, L.; Blake, P.; Schedin, F.; Mayorov, A.S.; Yuan, S.; et al. Fluorographene: A Two-Dimensional Counterpart of Teflon. *Small* **2010**, *6*, 2877–2884. [[CrossRef](#)]
31. Tang, X.; Debliquy, M.; Lahem, D.; Yan, Y.; Raskin, J.-P. A Review on Functionalized Graphene Sensors for Detection of Ammonia. *Sensors* **2021**, *21*, 1443. [[CrossRef](#)]
32. Liu, Y.; Shi, T.-T.; Chen, T.; He, W.-J.; Chen, M.-M.; Cao, D. The Naked-Eye NH₃ Sensor Based on Fluorinated Graphene. *Sensors Actuators B Chem.* **2019**, *281*, 789–794. [[CrossRef](#)]
33. Katkov, M.V.; Sysoev, V.I.; Gusel'nikov, A.V.; Asanov, I.P.; Bulusheva, L.G.; Okotrub, A.V. A Backside Fluorine-Functionalized Graphene Layer for Ammonia Detection. *Phys. Chem. Chem. Phys.* **2015**, *17*, 444–450. [[CrossRef](#)]
34. Yoon, T.; Jun, J.; Kim, D.Y.; Pourasad, S.; Shin, T.J.; Yu, S.U.; Na, W.; Jang, J.; Kim, K.S. An Ultra-Sensitive, Flexible and Transparent Gas Detection Film Based on Well-Ordered Flat Polypyrrole on Single-Layered Graphene. *J. Mater. Chem. A* **2018**, *6*, 2257–2263. [[CrossRef](#)]
35. Liang, X.; Sperling, B.A.; Calizo, I.; Cheng, G.; Hacker, C.A.; Zhang, Q.; Obeng, Y.; Yan, K.; Peng, H.; Li, Q.; et al. Toward Clean and Crackless Transfer of Graphene. *ACS Nano* **2011**, *5*, 9144–9153. [[CrossRef](#)]
36. Ferrari, A.C.; Basko, D.M. Raman Spectroscopy as a Versatile Tool for Studying the Properties of Graphene. *Nat. Nanotechnol.* **2013**, *8*, 235–246. [[CrossRef](#)]
37. Ferrari, A.C.; Meyer, J.C.; Scardaci, C.; Casiraghi, C.; Lazzeri, M. Raman Spectrum of Graphene and Graphene Layers. *Phys. Rev. Lett.* **2006**, *97*, 187401. [[CrossRef](#)]
38. Simon, L.; Bena, C.; Vonau, F.; Aubel, D.; Nasrallah, H.; Habar, M.; Peruchetti, J.C. Symmetry of Standing Waves Generated by a Point Defect in Epitaxial Graphene. *Eur. Phys. J. B* **2009**, *69*, 351–355. [[CrossRef](#)]
39. Lu, G.; Ocola, L.E.; Chen, J. Reduced Graphene Oxide for Room-Temperature Gas Sensors. *Nanotechnology* **2009**, *20*, 445502. [[CrossRef](#)]
40. Gautam, M.; Jayatissa, A.H. Gas Sensing Properties of Graphene Synthesized by Chemical Vapor Deposition. *Mater. Sci. Eng. C* **2011**, *31*, 1405–1411. [[CrossRef](#)]
41. Romero, H.E.; Joshi, P.; Gupta, A.K.; Gutierrez, H.R.; Cole, M.W.; Tadigadapa, S.A.; Eklund, P.C. Adsorption of Ammonia on Graphene. *Nanotechnology* **2009**, *20*, 245501. [[CrossRef](#)] [[PubMed](#)]
42. Attard, G.; Barnes, C. *Surface*; Oxford University Press: Oxford, UK, 1998.

43. Wongwiriyan, W.; Inoue, S.; Honda, S.; Katayama, M. Adsorption Kinetics of NO₂ on Single-Walled Carbon Nanotube Thin-Film Sensor. *Jpn. J. Appl. Phys.* **2008**, *47*, 8145–8147. [[CrossRef](#)]
44. Wongwiriyan, W.; Honda, S.; Konishi, H.; Mizuta, T.; Ikuno, T.; Ito, T.; Maekawa, T.; Suzuki, K.; Ishikawa, H.; Oura, K.; et al. Single-Walled Carbon Nanotube Thin-Film Sensor for Ultrasensitive Gas Detection. *Jpn. J. Appl. Phys.* **2005**, *44*, L482–L484. [[CrossRef](#)]
45. Wani, I.H.; Jafri, S.H.M.; Warna, J.; Hayat, A.; Li, H.; Shukla, V.A.; Orthaber, A.; Grigoriev, A.; Ahuja, R.; Leifer, K. A Sub 20 Nm Metal-Conjugated Molecule Junction Acting as a Nitrogen Dioxide Sensor. *Nanoscale* **2019**, *11*, 6571–6575. [[CrossRef](#)]
46. Zhang, Y.-H.; Chen, Y.-B.; Zhou, K.-G.; Liu, C.-H.; Zeng, J.; Zhang, H.-L.; Peng, Y. Improving Gas Sensing Properties of Graphene by Introducing Dopants and Defects: A First-Principles Study. *Nanotechnology* **2009**, *20*, 185504. [[CrossRef](#)]
47. Paul, R.K.; Badhulika, S.; Saucedo, N.M.; Mulchandani, A. Graphene Nanomesh as Highly Sensitive Chemiresistor Gas Sensor. *Anal. Chem.* **2012**, *84*, 8171–8178. [[CrossRef](#)]
48. Li, J.; Lu, Y.; Ye, Q.; Cinke, M.; Han, J.; Meyyappan, M. Carbon Nanotube Sensors for Gas and Organic Vapor Detection. *Nano Lett.* **2003**, *3*, 929–933. [[CrossRef](#)]